# Characterization of a charge-coupled device array for Bragg spectroscopy

Paul Indelicato, Eric-Olivier Le Bigot, and Martino Trassinelli[a)]
*Laboratoire Kastler Brossel, Unité Mixte de Recherche du CNRS n° 8552, Université Pierre et Marie Curie, Case 74, 4 Place Jussieu, F-75005 Paris, France*

Detlev Gotta and Maik Hennebach
*Institut für Kernphysik, Forschungszentrum Jülich, D-52425 Jülich, Germany*

Nick Nelms
*Space Research Center, Department of Physics and Astronomy, University of Leicester, University Road, Leicester LE1 7RH, United Kingdom*

Christian David and Leopold M. Simons
*Paul Scherrer Institut, CH-5232 Villigen, Switzerland*

(Received 21 November 2005; accepted 15 March 2006; published online 28 April 2006)

The average pixel distance as well as the relative orientation of an array of six charge-coupled device (CCD) detectors have been measured with accuracies of about 0.5 nm and 50 $\mu$rad, respectively. Such a precision satisfies the needs of modern crystal spectroscopy experiments in the field of exotic atoms and highly charged ions. Two different measurements have been performed by illuminating masks in front of the detector array by remote sources of radiation. In one case, an aluminum mask was irradiated with x rays, and in a second attempt, a nanometric quartz wafer was illuminated by a light bulb. Both methods gave consistent results with a smaller error for the optical method. In addition, the thermal expansion of the CCD detectors was characterized between −105 and −40 °C. © *2006 American Institute of Physics.* [DOI: 10.1063/1.2194485]

## I. INTRODUCTION

Charge-coupled devices (CCDs) are ideally suited as detectors for x-ray spectroscopy in the few keV range because of excellent energy resolution and the inherent two-dimensional spatial information. In particular, they can be used as focal-plane detectors of Bragg crystal spectrometers for studies of characteristic x radiation from exotic atoms with ultimate energy resolution.[1]

The detector described in this work was set up for a bent crystal spectrometer used in three ongoing experiments at the Paul Scherrer Institut: the measurement of the charged pion mass,[2,3] the determination of the strong-interaction shift and width of the pionic hydrogen ground state,[4,5] and highly charged ion spectroscopy.[6] The detector is made of an array of two vertical columns of three CCDs each[7] (Fig. 1). Each device has $600\times600$ square pixels with a nominal dimension of 40 $\mu$m at room temperature. Each pixel is realized by an open-electrode structure. For this reason, the dimension characterizing the detector is rather the average distance between pixel centers than the size of the individual pixel.

As the CCD is usually operated at −100 °C, the knowledge of the interpixel distance at the working temperature is essential for crystal spectroscopy, because any angular difference is determined from a measured position difference between Bragg reflections. Furthermore, for an array like the one described here, the relative orientation of the CCDs has to be known at the same level of accuracy as the average pixel distance.

A first attempt to determine the relative positions has been made using a wire-eroded aluminum mask illuminated by sulphur fluorescence x rays produced by means of an x-ray tube. The alignment of the mask pattern made it possible to estimate the relative CCD position with an accuracy of about 0.05–0.1 pixel and the relative rotation to slightly better than 100 $\mu$rad.[8] In order to obtain, in addition, a precise value for the average pixel distance, a new measurement was set up using a high-precision quartz wafer in front of the CCD illuminated with visible light. Using this method, the relative CCD devices' position was evaluated with an accuracy of about 0.02 pixel. The temperature dependence of the pixel distance was also determined.

Section II is dedicated to the description of the optical measurement setup. In Sec. III, we describe the measurement of the pixel distance. In Sec. IV we present the measurement of the CCD orientation using the aluminum mask (Sec. IV A) and the quartz mask (Sec. IV B). In Sec. V we describe the measurement of the interpixel distance temperature dependence.

## II. SETUP OF THE OPTICAL MEASUREMENT

The quartz wafer is an optical cross grating manufactured by the Laboratory of Micro- and Nanotechnology of the Paul Scherrer Institut. The cross grating pattern is generated by electron-beam lithography using a Leica LION-LV1

[a)]Author to whom correspondence should be addressed; electronic mail: martino.trassinelli@spectro.jussieu.fr

 

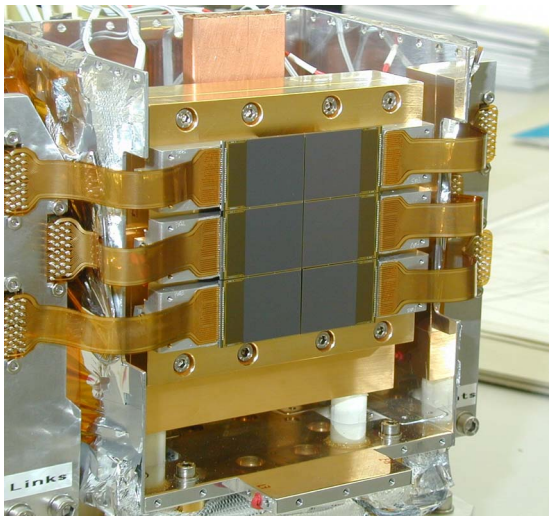

FIG. 1. Array of six CCD devices mounted on the cold head Ref. 7.

lithography tool with laser interferometer controlled sample stage with an increment of 2.5 nm. The grating is 40 mm wide and 70 mm high. It is composed of vertical and horizontal lines of 50 $\mu$m thickness separated from each other by 2 mm (Fig. 2). The accuracy of the cross grating in terms of linearity is essentially determined by the flatness of the interferometer mirrors. To determine this error, the cross grating was replaced into the lithography tool after rotating it by 180°, and the position of the intersection points along the outer lines was determined in scanning electron microscopy mode. This way, the linearity errors caused by the residual curvature of the interferometer mirrors along the horizontal and vertical cross grating lines could be mapped. The absolute accuracy of this well established method is typically better than 100 nm, the error is given by thermal drift of the lithography tool during exposure and inspection of the cross grating pattern. We found the linearity of the lines to be of order 0.05 $\mu$m in the horizontal direction. In the vertical direction, the lines become slightly parabolic with a maximum deviation of 0.15 $\mu$m from the average value (Fig. 3).

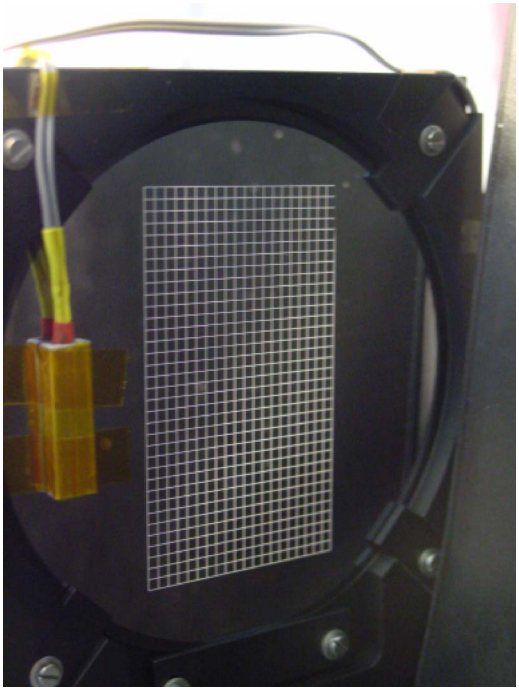

FIG. 2. Quartz wafer illuminated by light. The spacing of the grating is 2 mm both vertically and horizontally.

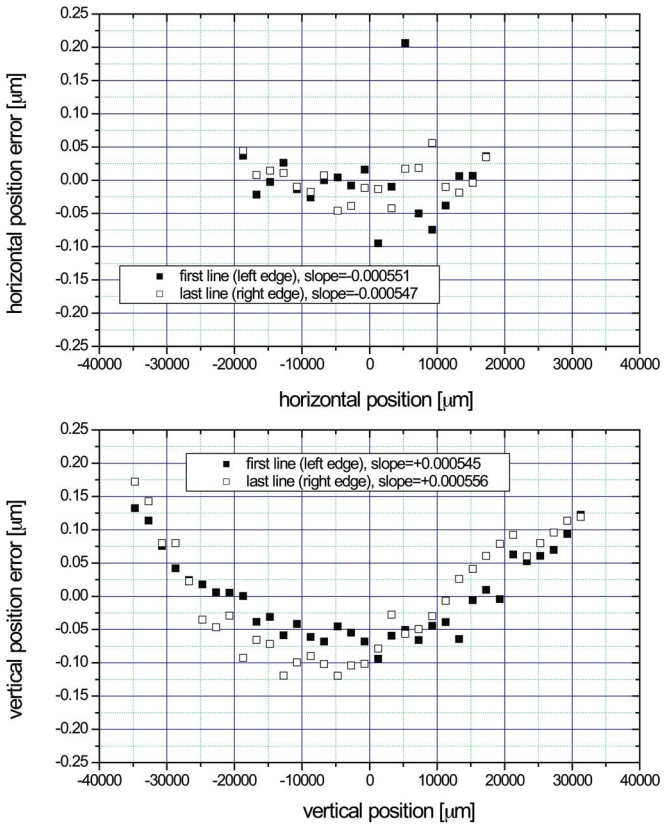


FIG. 3. Linearity of the grating in horizontal direction (top) and vertical direction (bottom).

The wafer was positioned 37 mm in front of the CCD array. It was illuminated with short light pulses using a point-like light source, which was approximated by a collimator of 1 mm in diameter located in front of a light bulb at a distance of 6.43 m from the CCDs to reduce parallax effects distorting the wafer image (Figs. 4 and 5). The wafer temperature was monitored and remained at room temperature during the measurements. The integration time per picture was 10 s with the bulb shining for 6 s for each selected temperature of the CCDs. The temperature was varied between −105 and −40 °C.

## III. MEASUREMENT OF THE AVERAGE PIXEL DISTANCE

For the determination of the pixel distance, a simultaneous linear fit of two adjacent lines was performed under the constraint that the two lines are parallel.

After cutting out the crossing points, the diffraction pattern of the straight sections linking them (zones) was fitted to

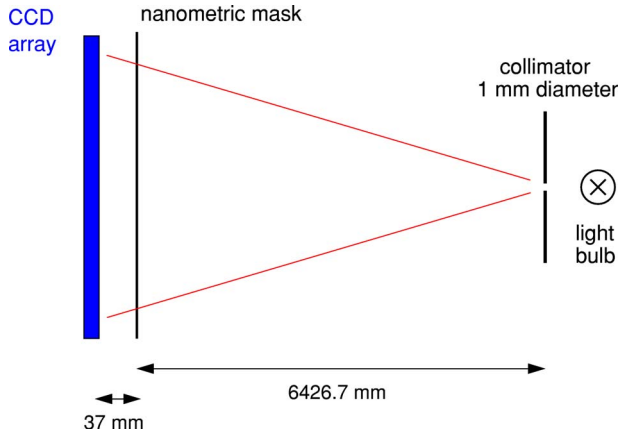


FIG. 4. Scheme of the experimental setup.

a superposition of five Gaussian profiles: central peak, first and second side maxima, and left and right backgrounds (Figs. 6 and 7). The parabolic shape of the grating was taken into account in the analysis of the images recorded with the detector.

For the fit of two parallel lines we have to consider two sets of data at the same time: $(x1_i, y1_i, \Delta y1_i)$ and $(x2_i, y2_i, \Delta y2_i)$, and the lines are described by the equations:

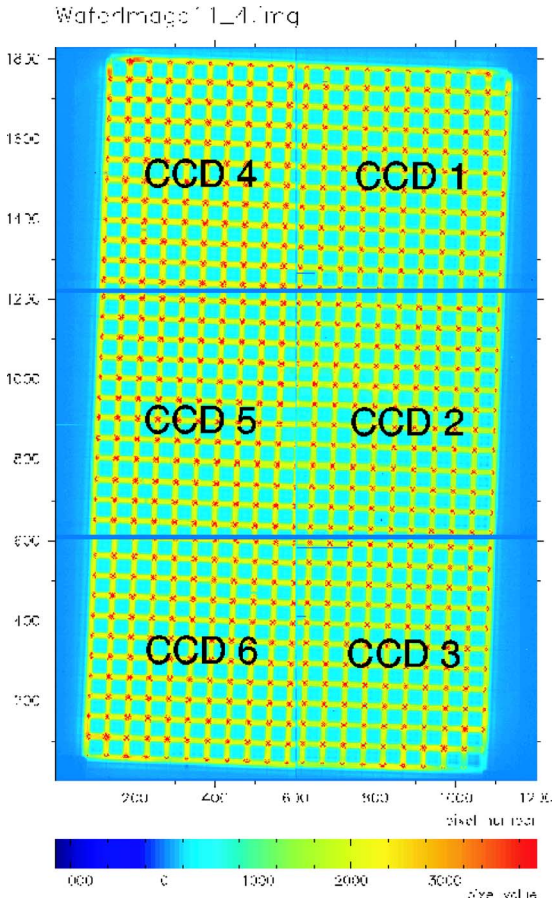


FIG. 5. Image of the quartz wafer as seen without correcting for the relative positions of the CCDs.

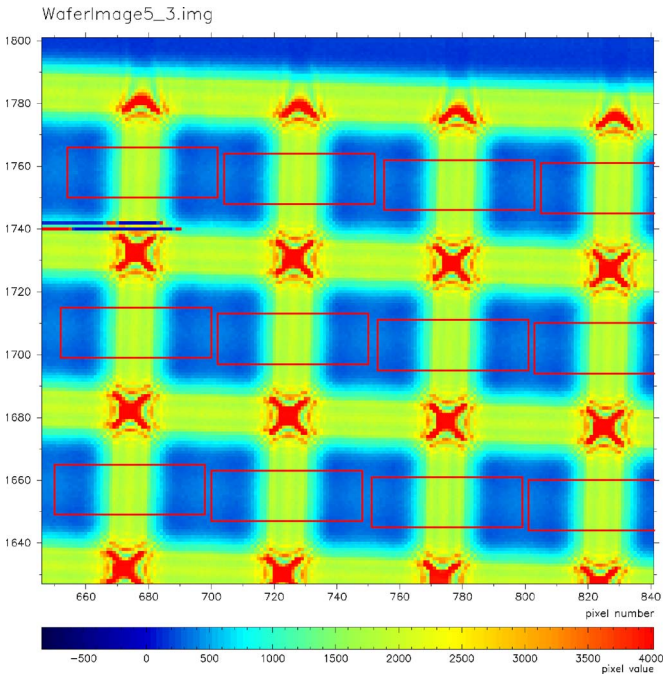


FIG. 6. Selection of the line fitting zones on the wafer image materialized by solid line rectangles.

$$\begin{cases} y1 = a1 + bx1, \\ y2 = a2 + bx2. \end{cases} \tag{1}$$

The best determination of the parameters $a1$, $a2$, and $b$ is obtained by minimization of the $\chi^2$ merit function following the same procedure as described in Ref. 9. In this case, the $\chi^2$ merit function is

$$\chi^2(a1,a2,b) = \sum_{i=1}^{N_1} \left( \frac{y1_i - a1 - bx1_i}{\Delta y1_i} \right)^2 + \sum_{i=1}^{N_2} \left( \frac{y2_i - a2 - bx2_i}{\Delta y2_i} \right)^2. \tag{2}$$

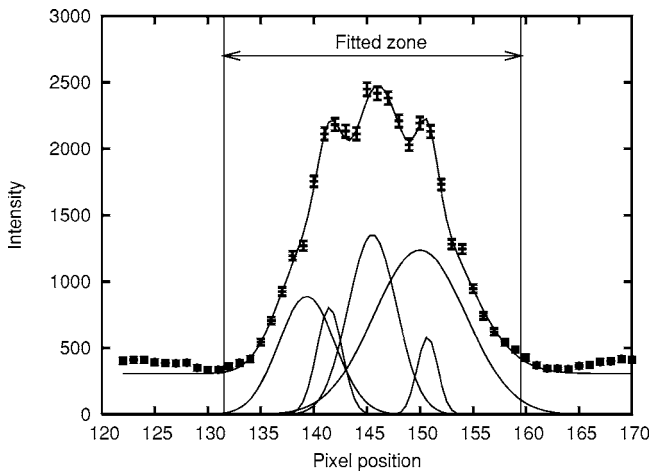


FIG. 7. Intensity profile of one pixel row of a selected zone. The line position is defined by using the average of the three central profiles. The other two profiles, normally characterized by a larger width, strongly depend on the background, i.e., on the illumination conditions of the selected zones.

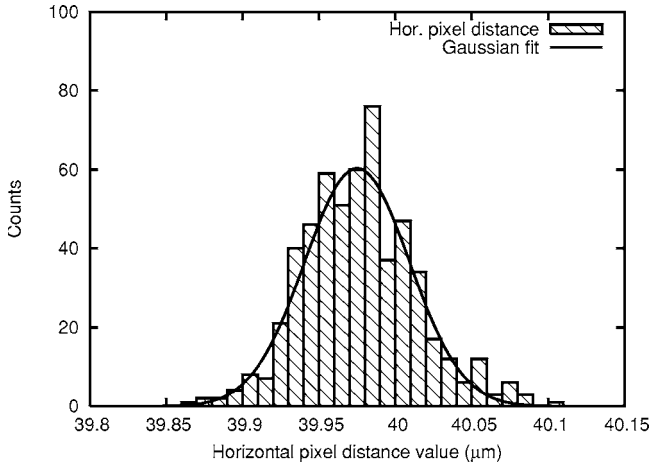


FIG. 8. Distribution of the horizontal pixel distance in CCD 3 as obtained from pairs of selected zones.

Considering two parallel lines that are at a distance $L$ (in $\mu$m) on the CCD, the average pixel distance is obtained from the formula

$$\text{pixel distance} = \frac{L}{|a1 - a2|\cos(\arctan b)} = L\frac{\sqrt{1+b^2}}{|a1 - a2|}. \quad (3)$$

The presence of the cosine term takes into account the fact that the lines are generally not parallel to the CCD edge. The detailed formulas for the $\chi^2$ minimization are presented in Appendix A.

For each CCD, we obtained about 180 independent evaluations of the pixel distance from straight sections of different line pairs. The average value of the pixel distance was obtained by a Gaussian fit to the histogram obtained from individual values (Figs. 8 and 9). Two series of images were available, and the final value was calculated from the sum of the two distributions.

It is interesting to observe that the vertical and horizontal distributions have different dispersions (Figs. 8 and 9 and Table I). The horizontal pixel distance distribution is characterized by a full width at half maximum (FWHM) of 80 nm,

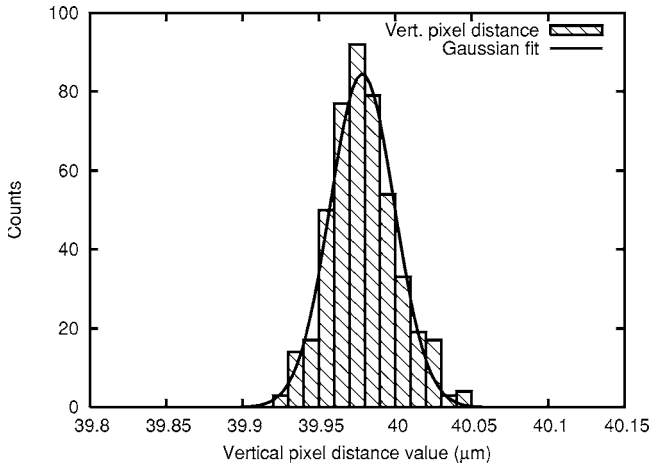


FIG. 9. Distribution of the vertical pixel distance in CCD 3 as obtained from pairs of selected zones.

TABLE I. Results of a Gaussian fit to the horizontal and vertical pixel distance distributions. The fabrication accuracy of the quartz wafer contributes with additionally 0.1 nm to the average pixel distance.

| CCD | Horizontal distance ($\mu$m) | FWHM ($\mu$m) | $\chi^2$ |
|---|---|---|---|
| 1 | 39.9778±0.0018 | 0.0820±0.0035 | 1.11 |
| 2 | 39.9743±0.0018 | 0.0810±0.0033 | 1.26 |
| 3 | 39.9751±0.0018 | 0.0808±0.0033 | 1.41 |
| 4 | 39.9753±0.0017 | 0.0808±0.0032 | 1.16 |
| 5 | 39.9744±0.0017 | 0.0856±0.0031 | 1.01 |
| 6 | 39.9777±0.0018 | 0.0913±0.0031 | 1.20 |
| Weighted average 39.9764±0.0009 without CCDs 2 and 5 line fits | | | |
| CCD | Vertical distance ($\mu$m) | FWHM ($\mu$m) | $\chi^2$ |
| 1 | 39.9766±0.0012 | 0.0504±0.0022 | 1.05 |
| 2 | 39.9787±0.0008 | 0.0420±0.0014 | 0.88 |
| 3 | 39.9785±0.0010 | 0.0496±0.0019 | 0.68 |
| 4 | 39.9769±0.0009 | 0.0450±0.0016 | 0.62 |
| 5 | 39.9781±0.0007 | 0.0472±0.0013 | 0.52 |
| 6 | 39.9787±0.0007 | 0.0423±0.0014 | 0.66 |
| Weighted average 39.9779±0.0004 without CCDs 2 and 5 line fits | | | |

compared to 50 nm for the vertical one. Accordingly, the error on the Gaussian peak position for the vertical distance is half that for the horizontal one (0.9 and 1.8 nm, respectively). We have no clear-cut explanation for this difference. It is unlikely that this difference could come from the accuracy of the mask fabrication. As seen from Fig. 3, the line distances show similar fluctuations in the order of 0.05 $\mu$m for both directions and they should produce a dispersion of about 0.05 $\mu$m/50=1 nm on the vertical and horizontal pixel distances (50 is the average number of pixels between two lines in the wafer image).

The CCD devices were fabricated using a 0.5 $\mu$m technology, which means that the uncertainty over the full size is 0.5 $\mu$m (at room temperature). Such an inaccuracy could introduce an average difference of order 0.8 nm for the interpixel distance of various CCDs. This assumption was tested applying *student's t-test*[9] to distributions from different CCDs. The only significant difference in the obtained distributions comes from CCD 2 and CCD 5. However, for these two CCDs we observe a parasitic image of the mask superimposed on the normal one, probably due to a reflection between the detector and the mask itself. Therefore, the final value of the pixel distance is given by the weighted average of the individual CCD values excluding CCD 2 and CCD 5 (Table I).

As pointed out in Sec. II the overall precision of the quartz wafer is better than ±0.0001 mm over its full width of 40 mm. Hence, the uncertainty of the wafer grid contributes on average 0.1 $\mu$m/1000=0.1 nm/pixel. As horizontal and vertical pixel distances are in good agreement, a weighted average is calculated. Taking the wafer uncertainty of 0.1 nm into account, the average pixel distance reads 39.9775±0.0005±0.0001 $\mu$m, where the nominal value is 40 $\mu$m.

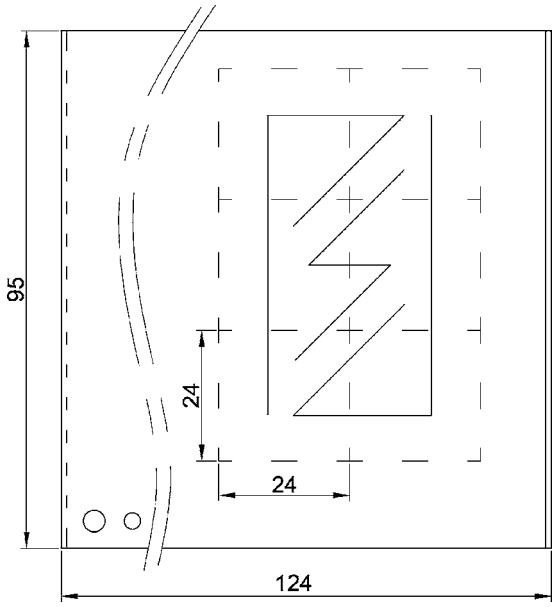


FIG. 10. Wire-eroded aluminum mask for the CCD alignment.

## IV. MEASUREMENT OF THE RELATIVE ORIENTATION OF THE CCDS

### A. X-ray method

An aluminum mask was installed 37 mm in front of the CCD array (Fig. 10); this mask has a slit pattern chosen to provide an unambiguous connection between all CCDs (Fig. 11). The mask has a thickness of 1 mm, the slits are wire eroded with a width of approximately 0.1 mm. The deviation from linearity of the slits is up to 50 $\mu$m over the full length. The detector array, shielded by the mask, was irradiated with sulphur x rays of 2.3 keV produced with the help of an x-ray tube; this energy is low enough to keep charge splitting effects small.[7] The sulphur target was placed at about 4 m from the detector. A collimator with a diameter of 5 mm was placed close to the target to provide a pointlike source. Target and collimator were mounted inside a vacuum tube connected to the detector's cryostat without any window. The sulphur plate itself was irradiated through a Kapton window. In total, about 600 000 x-ray events were collected.

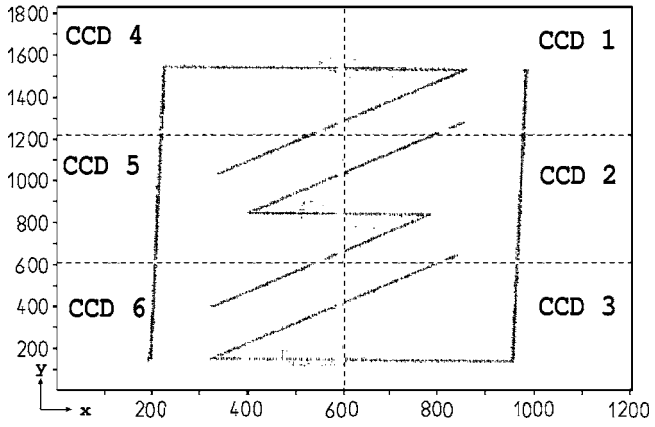


FIG. 11. Pattern produced by sulphur $K\alpha$ radiation excited by means of an x-ray tube (axis not to scale).

TABLE II. CCD position corrections (relative to CCD 3) from the mask measurement using sulphur fluorescence radiation.

| CCD | $\Delta x$ (pixels) | $\Delta y$ (pixels) | $\Delta\Theta$ (mrad) |
|---|---|---|---|
| CCD3-CCD1 | −2.818±0.022 | 22.264±0.077 | 0.197±0.078 |
| CCD3-CCD2 | −1.049±0.015 | 10.901±0.085 | 0.522±0.062 |
| CCD3-CCD3 | 0.000±0.000 | 0.000±0.000 | 0.000±0.000 |
| CCD3-CCD4 | −14.347±0.046 | 20.808±0.075 | 1.577±0.084 |
| CCD3-CCD5 | −14.597±0.043 | 12.265±0.064 | 2.940±0.109 |
| CCD3-CCD6 | −16.487±0.040 | 1.173±0.052 | 6.328±0.101 |

The relative rotations of the CCDs are determined by performing linear fits to sections of the mask slit images. Because of the slit arrangement, CCD 3 (CCD 6 would be equivalent) is the best choice to serve as reference frame. In this case, the relative rotations of CCDs 1, 2, and 6 are established directly. The values for CCD 4 and CCD 5 are the weighted average of results with CCD 1 and CCD 6 as intermediate steps.

The fit is done by calculating the center of gravity (COG) for each CCD row (or column for fitting a horizontal line) and then making a linear regression through them. The error of the COGs is based upon a rectangular distribution with a width equal to the width of the slits of the mask. With $N$ as the number of events and $w$ as the slit width, $\Delta_{\mathrm{COG}} = w/\sqrt{12}\sqrt{N}$. A width $w$ of 4 pixels for the horizontal/vertical lines and 6 pixels for the diagonals is assumed. From the inclinations (in mrad) of the mask slits relative to the perfect horizontal, vertical or diagonal (45°), the rotations $\Delta\Theta$ of individual CCDs are calculated. Results (relative to CCD 3) are given in Table II.

After the rotations have been determined and corrected, the lines were fitted again to determine the crossing points of each slit with the CCD edge. The relative offsets $\Delta x$ and $\Delta y$ can be determined only if there are at least two lines crossing from one CCD to the other (Fig. 12). With CCD 3 as the starting point, the only other CCD fulfilling this condition is CCD 6. The position of all other CCDs has to be calculated relative to all CCDs shifted so far. The correct order for this is CCD 2, then CCD 5, CCD 1, and CCD 4.

The correct values for the vertical offsets follow from the condition that both lines should continue from one CCD to the other (CCD A and CCD B in Fig. 12). For case (i) in

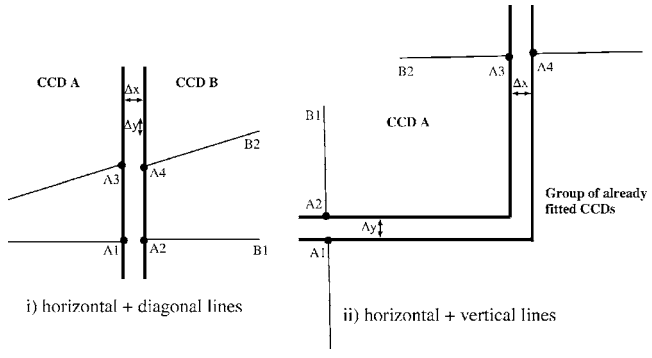


FIG. 12. Definition of crossing points for the determination of the relative offsets of the CCDs.

Fig. 12, one horizontal and one diagonal line:

$$\begin{cases} A_1 + \Delta y + B_1 \Delta x = A_2, \\ A_3 + \Delta y + B_2 \Delta x = A_4, \end{cases} \tag{4}$$

where $A_i$ are the $y$ coordinate of the crossing point between the lines of equation $y = B_i x + (\text{constant})$ and the CCD edge. From this, one derives

$$\Delta x = \frac{(A_2 - A_4) - (A_1 - A_3)}{B_1 - B_2}, \tag{5}$$

and the associate error is

$$\delta(\Delta x) = \left\{ \frac{(\delta A_1)^2 + (\delta A_2)^2 + (\delta A_3)^2 + (\delta A_4)^2}{(B_1 - B_2)^2} + \frac{[(\delta B_1)^2 + (\delta B_2)^2](A_2 - A_4 - A_1 + A_3)^2}{(B_1 - B_2)^4} \right\}^{1/2}. \tag{6}$$

For case (ii), one horizontal and one vertical line,

$$\begin{cases} A_1 + \Delta x + B_1 \Delta y = A_2, \\ A_3 + \Delta y + B_2 \Delta x = A_4, \end{cases} \tag{7}$$

note that $B_1$ is defined as $x = B_1 y + (\text{constant})$. Here, the equations are

$$\Delta x = \frac{A_1 - A_2 - B_1(A_3 - A_4)}{B_1 B_2 - 1}, \tag{8}$$

$$[\delta(\Delta x)]^2 = \frac{(\delta A_1)^2 + (\delta A_2)^2 + (\delta B_1)^2[(\delta A_3)^2 + (\delta A_4)^2]}{(B_1 B_2 - 1)^2} + (\delta B_1)^2 \left\{ \frac{A_4 - A_3}{B_1 B_2 - 1} - \frac{B_2[A_1 - A_2 - B_1(A_3 - A_4)]}{(B_1 B_2 - 1)^2} \right\}^2 + (\delta B_2)^2 \left\{ \frac{B_1[A_1 - A_2 - B_1(A_3 - A_4)]}{(B_1 B_2 - 1)^2} \right\}^2. \tag{9}$$

Values for $\Delta y$ are derived by inserting $\Delta x$ in either of the starting equations Eq. (4). The final horizontal and vertical displacements (which depend on the previously determined set of rotations) are given in Table II.

The analysis of the mask data assumes that the slits on the mask are perfectly straight; the given uncertainties are then purely statistical. However, a detailed study of the vertical slit to the right (on CCD 1 to CCD 3) shows that the mechanical irregularities of the mask are big enough to be noticeable. Figure 13 shows the centers of gravity calculated for this slit subtracted from the fit through these points. Both the sudden jump (left arrow) and the inclination change (right arrow) are substructures on a scale of roughly 1/10 of a pixel (4 $\mu$m). This fits well with the mechanical accuracy of 5 $\mu$m quoted for the mask slits. Consequently, a further improvement in accuracy is not limited by statistics, but by the mechanical precision of the mask itself. More details may be found in Ref. 8.

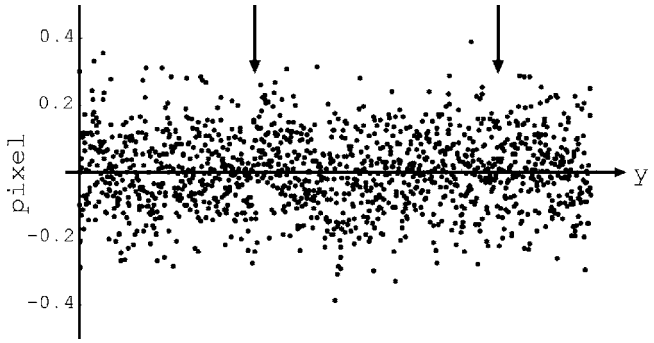


FIG. 13. Centers of gravity of the right vertical slit of the wire-eroded aluminum mask. Arrows indicate the two largest irregularities.

### B. Optical method

By using the nanometric quartz wafer, the precision for the CCD offsets was improved beyond 1/20 of the pixel width of 40 $\mu$m, which was envisaged for measuring the charged pion mass. The knowledge of the line positions on the wafer allows one to infer the relative position between pairs of CCDs from the image. As for x rays, the image, when visualized without position and rotation correction, shows discontinuities at the boundaries of adjacent CCDs: lines are not parallel, and a part of the mask image is missing due to the spatial separation of the CCDs (Fig. 14, bottom left). Again, one CCD has to be chosen as a reference.

The unambiguous calculation of relative horizontal and

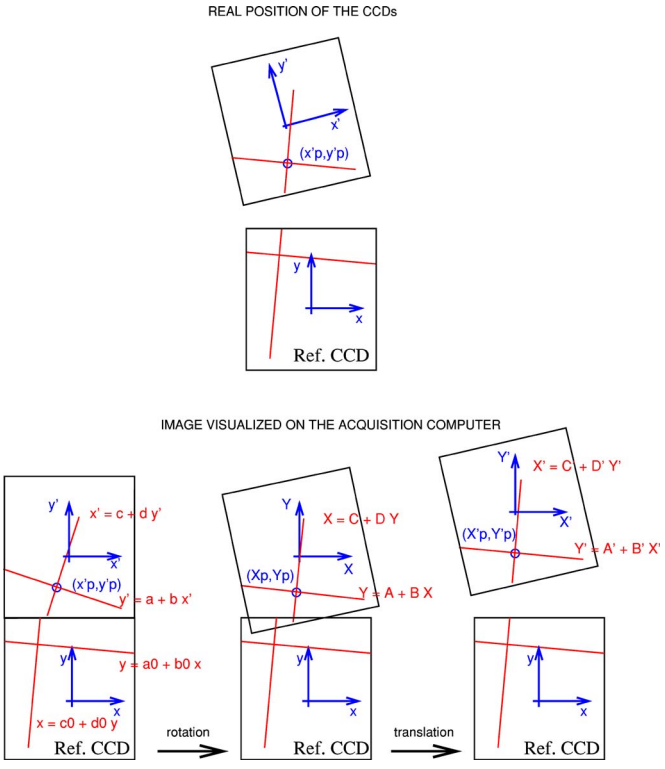


FIG. 14. Scheme of the transformation used in obtaining the orientation and shift between CCDs. In the top part, the real position of the CCDs is shown together with one crossing of the quartz grid. In the lower part, the transformation from the individual CCD coordinates (left) to the real relative position with respect to the reference CCD is displayed. The rotation is first performed, (middle) and then the shift is adjusted from the known geometry of the grid (right).

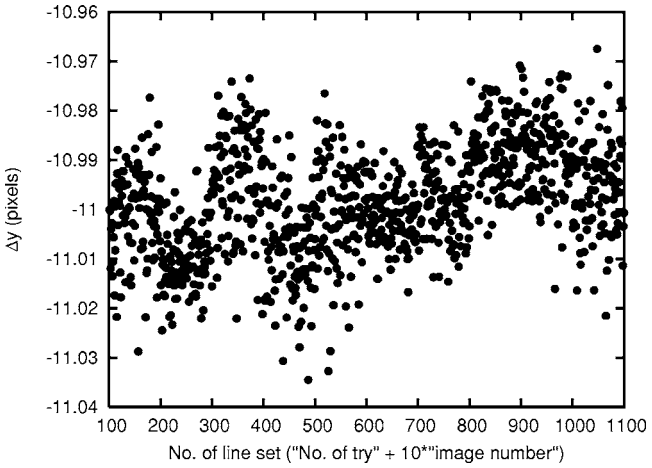


FIG. 15. Distribution of the relative shift $\Delta y$ (gap) for CCD 3 relative to reference CCD 2 for various crossing points. Each point corresponds to a value of $\Delta y$ obtained for a set of line pairs. For each of the ten images, 100 sets of line pairs have been randomly chosen. The slope with time (corresponding approximately to the "No. of line set" axis) may be due to the CCD array not reaching the thermal equilibrium.

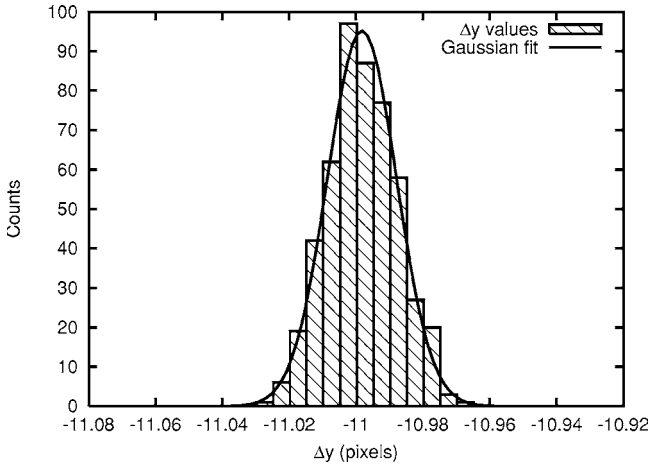


FIG. 16. Projection of the $\Delta y$ distribution. A Gaussian fit yields the most likely value and an estimate for the uncertainty of $\Delta y$.

vertical shifts ($\Delta x$ and $\Delta y$) and rotation ($\Delta\Theta$) of two CCDs requires the information coming from at least one pair of perpendicularly crossing lines per CCD. Using the line parameters, it is possible to build a function depending upon $\Delta x$, $\Delta y$, and $\Delta\Theta$, which is minimal when the shift and rotation values are optimal. The idea is to compare the coordinates of a crossing point using the reference frame of the reference CCD $(x_p, y_p)$ and of the selected CCD $(x_p', y_p')$. The values of $\Delta x$ and $\Delta y$ are unequivocally determined by first applying a rotation of the coordinate system of the selected CCD around the CCD center. The value of the rotation angle $\Delta\Theta$ is chosen to have the lines parallel to the ones of the reference CCD (Fig. 14, bottom-middle side). In this new frame, the coordinates $(X_p, Y_p)$ of the crossing point depend on the line parameters and on the value of $\Delta\Theta$. The differences $X_p - x_p$ and $Y_p - y_p$ provide exactly the shift values $\Delta x$ and $\Delta y$. A function $F$ may be defined as

$$F(\Delta x, \Delta y, \Delta\Theta) = (X_p - x_p - \Delta x)^2 + (Y_p - y_p - \Delta y)^2. \quad (10)$$

In the ideal case, $F=0$, the values of $\Delta x$, $\Delta y$, and $\Delta\Theta$ are the correct ones. In reality we assume that, for a selected set of lines, the best estimate of $\Delta x$, $\Delta y$, and $\Delta\Theta$ is found when $F$ is minimal. The full expression used for $F$ is given in Appendix B.

A whole set of values was obtained by randomly selecting line pairs. For different choices of line pairs, different values are obtained for the position parameters. Hence, the final values of $\Delta x$, $\Delta y$, and $\Delta\Theta$ are given again by a Gaussian fit to the distribution of the individual values. The accuracy of this method can be increased by forcing the simultaneous minimization of coordinate differences for several crossing points instead of only one. Here, four crossing points and a set of 100 different choices (Fig. 15) of line pairs were used. In this case the function $F$ reads

$$F(\Delta x, \Delta y, \Delta\Theta) = \sum_{i=1}^{4} (X_p^i - x_p^i - \Delta x)^2 + (Y_p^i - y_p^i - \Delta y)^2, \quad (11)$$

where $i=1-4$ corresponds to the crossing point number arbitrarily ordered. Figure 16 shows the distribution data for $\Delta y$ obtained for the full set of line pairs.

The final result for the relative CCD positions was obtained from three series of ten images each: two at $-100$ °C and one at $-105$ °C. The precision for each series is around 0.001 pixels for $\Delta x$ and $\Delta y$, and 3 $\mu$rad for the relative rotation $\Delta\Theta$, and it can be reduced using a function $F$ with more crossing points. The systematic errors were estimated by comparing the results from the three series of data acquisition. However, the differences between values from different series are of order 0.01–0.03 pixels for $\Delta x$ and $\Delta y$, and 50 $\mu$rad for $\Delta\Theta$. This large spread, compared to the precision of each series, has two possible explanations: differences of the wafer illumination condition (affecting the line fit) or a mechanical change of the CCD array position during warming up and cooling of the detector. The second hypothesis is more likely, because only small differences were observed between the series at $-105$ °C and the first series at $-100$ °C, where no warming up between the two measurements was performed. In contrast, before the second series at $-100$ °C, the detector was at room temperature for a short period. This hypothesis is also confirmed by the observation of a small change in time of the $\Delta y$ values in Fig. 15, where a significant change is observed between points obtained from different images. These differences could be attributed to a mechanical change in time due to the not yet attained thermal equilibrium of the CCD array during the measurement.

For each CCD, the final position and rotation parameters are calculated as the average of the three series (Table III). The systematic effect from the temperature difference of the image series is negligibly small compared to the spread of values. The systematic error is estimated using the standard deviation formula for a set of values. For CCD 4, only one

TABLE III. CCD relative position and orientation with CCD 2 as reference. The orientation of CCD 2 relative to itself provides a check of the validity of the measurement method.

| CCD | $\Delta x$ (pixels) | $\Delta y$ (pixels) | $\Delta\Theta$ (mrad) |
|---|---|---|---|
| CCD2-CCD1 | −1.251±0.029 | 11.404±0.023 | −0.587±0.035 |
| CCD2-CCD2 | 0.000±0.000 | 0.000±0.000 | −0.002±0.003 |
| CCD2-CCD3 | 0.509±0.012 | −11.021±0.021 | −0.677±0.074 |
| CCD2-CCD4 | −12.850±0.041 | 10.279±0.023 | 0.801±0.130 |
| CCD2-CCD5 | −13.579±0.009 | 1.738±0.016 | 2.233±0.130 |
| CCD2-CCD6 | −15.963±0.041 | −9.435±0.021 | 5.530±0.011 |

series of measurements was available. In this case, the largest value of all other CCDs was chosen.

The fabrication of the grating introduces a systematic error due to the slightly parabolic shape of the vertical lines (Fig. 3). The error is estimated to be of order of 9 $\mu$rad for $\Delta\Theta$ and 0.009 pixels for $\Delta x$ for CCD 1, CCD 3, CCD 4, and CCD 6, which is negligible compared with other systematic errors.

The values presented in Table III are in very good agreement with the results obtained using the aluminum mask, taking into account the different reference CCDs. As an example, for the $\Delta x$ shift between CCD 5 and CCD 2 we obtain $-13.548\pm0.045$ pixels with the x-ray method and $-13.579\pm0.009$ pixels with the optical method.

## V. TEMPERATURE DEPENDENCE OF THE PIXEL DISTANCE

For the determination of the temperature dependence, images between −105 and −40 °C were acquired. For each condition the same analysis method as described in Sec. III was applied. As expected, the pixel distance increases with increasing temperature except for the vertical pixel distance at −40 °C (Table IV). This effect may be caused by the high CCD read-noise level at this temperature. The values obtained at −40 °C have been ejected for the measurement of the temperature dependence.

The average of the thermal expansion coefficient is obtained by a simple linear extrapolation of the data between −105 and −60 °C. The results are $(2.8\pm1.0)\times10^{-6}$ K$^{-1}$ for the horizontal distance and $(1.3\pm0.4)\times10^{-6}$ K$^{-1}$ for the vertical distance. These values are in the range of the thermal expansion coefficient of silicon, the CCD substrate material, and invar, the metallic support material for the temperatures considered: literature values are $(0.8-1.6)\times10^{-6}$ K$^{-1}$ for silicon[10] and $(1-2)\times10^{-6}$ K$^{-1}$ for invar.[11]

TABLE IV. Pixel distance values at different detector temperatures.

| Temperature (°C) | Horizontal pixel distance ($\mu$m) | Vertical pixel distance ($\mu$m) |
|---|---|---|
| −105 | 39.9796±0.0014 | 39.9779±0.0006 |
| −100 | 39.9764±0.0009 | 39.9779±0.0004 |
| −80 | 39.9796±0.0020 | 39.9794±0.0006 |
| −60 | 39.9827±0.0017 | 39.9800±0.0006 |
| −40 | 39.9837±0.0013 | 39.9762±0.0010 |

## VI. DISCUSSION

We have demonstrated that the average interpixel distance of a CCD detector under operating conditions can be determined to an accuracy of 15 ppm. We obtain $39.9775\pm0.0006$ $\mu$m for the average pixel distance at a temperature of −100 °C, which deviates significantly from the nominal value of 40 $\mu$m. Also, the temperature dependence of the interpixel distance was studied and successfully compared to values found in the literature. The relative rotations and positions of the individual CCD devices of a $2\times3$ array have been measured to a precision of about 50 $\mu$rad and 0.02 pixel, respectively. The x-ray method was limited by the quality of the aluminum mask, i. e., by the accuracy of wire-eroding machine. With the nanometric quartz wafer no limitation occurs from the accuracy of the mask. The principal difficulty encountered in that case is the proper description of the diffraction pattern and, in particular, the control of the illumination. The accuracy achieved by this method fully satisfies the requirements of a recent attempt to measure the charged pion mass to about 1.5 ppm. The x-ray method and the optical method can be used for any CCD camera sensitive to x-ray and/or visible light radiations.

## ACKNOWLEDGMENT

Partial travel support for this experiment has been provided by the French–Swiss "programme d'action intégrée Germaine de Staël," contract number 07819NH.

## APPENDIX A: FORMULAS FOR FITTING WITH A PAIR OF PARALLEL LINES

In this appendix, we present mathematical formulas for linear fitting with a pair of parallel lines, i.e., for the minimization of the $\chi^2$ merit function defined in Eq. (2).

$\chi^2$ is minimized when its derivatives with respect to $a1$, $a2$, and $b$ vanish:

$$\begin{cases} 0=\dfrac{\partial\chi^2}{\partial a1}=-2\displaystyle\sum_{i=1}^{N_1}\dfrac{y1_i-a1-bx1_i}{\Delta y1_i^2}, \\ 0=\dfrac{\partial\chi^2}{\partial a2}=-2\displaystyle\sum_{i=1}^{N_2}\dfrac{y2_i-a2-bx2_i}{\Delta y2_i^2}, \\ 0=\dfrac{\partial\chi^2}{\partial b}=-2\left[\displaystyle\sum_{i=1}^{N_1}\dfrac{x1_i(y1_i-a1-bx1_i)}{\Delta y1_i^2}+\sum_{i=1}^{N_2}\dfrac{x2_i(y2_i-a2-bx2_i)}{\Delta y2_i^2}\right]. \end{cases} \tag{A1}$$

These conditions can be rewritten in a convenient form if we define the following sum:

$$S1 = \sum_{i=1}^{N_1} \frac{1}{\Delta y1_i^2}, \quad S1_x = \sum_{i=1}^{N_1} \frac{x1_i}{\Delta y1_i^2}, \tag{A2}$$

$$S1_y = \sum_{i=1}^{N_1} \frac{y1_i}{\Delta y1_i^2}, \tag{A3}$$

$$S1_{xx} = \sum_{i=1}^{N_1} \frac{x1_i^2}{\Delta y1_i^2}, \quad S1_{xy} = \sum_{i=1}^{N_1} \frac{x1_i y1_i}{\Delta y1_i^2}, \tag{A4}$$

$$S2 = \sum_{i=1}^{N_2} \frac{1}{\Delta y2_i^2}, \quad S2_x = \sum_{i=1}^{N_2} \frac{x2_i}{\Delta y2_i^2}, \tag{A5}$$

$$S2_y = \sum_{i=1}^{N_2} \frac{y2_i}{\Delta y2_i^2}, \tag{A6}$$

$$S2_{xx} = \sum_{i=1}^{N_2} \frac{x2_i^2}{\Delta y2_i^2}, \quad S2_{xy} = \sum_{i=1}^{N_2} \frac{x2_i y2_i}{\Delta y2_i^2}. \tag{A7}$$

With this definitions Eq. (A1) becomes

$$\begin{cases} a1S1 + bS1_x = S1_y, \\ a2S2 + bS2_x = S2_y, \\ a1S1_x + bS1_{xx} + a2S2_x + bS2_{xx} = S1_{xy} + S2_{xy}. \end{cases} \tag{A8}$$

The solution of these three equations with three unknowns is

$$\begin{cases} a1 = -\dfrac{S2S1_xS1_{xy} + S2S1_xS2_{xy} + S2_x^2S1_y - S2S1_{xx}S1_y - S2S2_{xx}S1_y - S1_xS2_xS2_y}{-S2S1_x^2 - S1S2_x^2 + S1S2S1_{xx} + S1S2S2_{xx}}, \\ a2 = -\dfrac{-S1S2_xS1_{xy} - S1S2_xS2_{xy} + S1_xS2_xS1_y - S1_x^2S2_y + S1S1_{xx}S2_y + S1S2_{xx}S2_y}{S2S1_x^2 + S1S2_x^2 - S1S2S1_{xx} - S1S2S2_{xx}}, \\ b = -\dfrac{S1S2S1_{xy} + S1S2S2_{xy} - S2S1_xS1_y - S1S2_xS2_y}{S2S1_x^2 + S1S2_x^2 - S1S2S1_{xx} - S1S2S2_{xx}}. \end{cases} \tag{A9}$$

## APPENDIX B: DEFINITION OF THE FUNCTION $F(\Delta x, \Delta y, \Delta\Theta)$

The exact form of $F$ in Eq. (10) can be deduced using simple algebraic equations and reference frame transformation formulas. If we take any pair of perpendicular lines in the reference CCD (see Fig. 14),

$$y = a_0 + b_0 x \quad \text{and} \quad x = c_0 + d_0 y, \tag{B1}$$

the coordinates $(x_p, y_p)$ from the line intersection can be calculated on the selected CCD. The parameters of these lines are deduced from the lines in the reference CCD [Eq. (B1)], taking into account the necessary change on $a_0$ and $c_0$ for the translation on the grating pattern:

$$\begin{pmatrix} x_p \\ y_p \end{pmatrix} : \begin{cases} x_p = c_0 + sy + d_0 y_p, \\ y_p = a_0 + sx + b_0 x_p. \end{cases} \tag{B2}$$

Here, $sx$ and $sy$ are the parameters of the translation that can be easily deduced from the wafer image. In this case we have

$$\begin{cases} x_p = \dfrac{c_0 + d_0(a_0 + sx) + sy}{1 - b_0 d_0}, \\ y_p = \dfrac{a_0 + b_0(c_0 + sy) + sx}{1 - b_0 d_0}. \end{cases} \tag{B3}$$

In the same way we can calculate the coordinates $(X_p, Y_p)$: the crossing point of the lines in the selected CCD after the $\Delta\Theta$ rotation. Before the rotation, the line coordinates on the selected CCD are

$$y' = a + bx' \text{ and } x' = c + dy'. \tag{B4}$$

After rotation around the CCD center $(X_C, Y_C)$ the line equations become (see Fig. 14)

$$Y = A + BX \text{ and } X = C + DY, \tag{B5}$$

where the line parameters are given by

$$A = \frac{a + bX_C - Y_C + (Y_C - bX_C)\cos\Delta\Theta - (X_C + bY_C)\sin\Delta\Theta}{\cos\Delta\Theta - b\sin\Delta\Theta} \tag{B6}$$

$$B = \frac{b\cos\Delta\Theta + \sin\Delta\Theta}{\cos\Delta\Theta - b\sin\Delta\Theta} \tag{B7}$$

$$C = \frac{c - X_C + dY_C + (X_C - dY_C)\cos\Delta\Theta + (Y_C + dX_C)\sin\Delta\Theta}{\cos\Delta\Theta + d\sin\Delta\Theta} \tag{B8}$$

$$D = \frac{d\cos\Delta\Theta - \sin\Delta\Theta}{\cos\Delta\Theta + d\sin\Delta\Theta}. \tag{B9}$$

With this reference change, the coordinates $(X_p, Y_p)$ are

$$\begin{cases} X_p = \dfrac{(bd-1)X_C - [c+ad+(bd-1)X_C]\cos\Delta\Theta + [a+bc+(bd-1)Y_C]\sin\Delta\Theta}{bd-1}, \\ Y_p = \dfrac{(bd-1)Y_C - [a+bc+(bd-1)Y_C]\cos\Delta\Theta + [c+ad+(bd-1)X_C]\sin\Delta\Theta}{bd-1}. \end{cases} \tag{B10}$$

The function $F$ is defined as

$$\begin{aligned} F(\Delta x,\Delta y,\Delta\Theta) &= (X_p - x_p - \Delta x)^2 + (Y_p - y_p - \Delta y)^2 \\ &= \left( \frac{1}{(bd-1)(b_0d_0-1)}\{(bd-1)(c_0 + a_0d_0 + d_0sx + sy - X_C + b_0d_0X_C) - (b_0d_0-1)[c+ad+(bd \right. \\ &\quad -1)X_C]\cos\Delta\Theta + (b_0d_0-1)[a+bc+(bd-1)Y_C]\sin\Delta\Theta\} - \Delta x \Big)^2 + \Big( \frac{1}{(bd-1)(b_0d_0-1)}\{(bd-1)(a_0 \\ &\quad + b_0c_0 + b_0sy + sx - Y_C + b_0d_0Y_C) - (b_0d_0-1)[a+bc+(bd-1)Y_C]\cos\Delta\Theta + (b_0d_0-1)[c+ad+(bd \\ &\quad \left. -1)Y_C]\sin\Delta\Theta\} - \Delta y \right)^2. \end{aligned} \tag{B11}$$


[1] D. Gotta, Prog. Part. Nucl. Phys. **52**, 133 (2004).
[2] Pion Mass Collaboration, PSI experiment proposal R-97.02 (1997).
[3] N. Nelms *et al.*, Nucl. Instrum. Methods Phys. Res. A **477**, 461 (2002).
[4] Pionic Hydrogen Collaboration, PSI experiment proposal R-98.01 (1998), http://pihydrogen.web.psi.ch
[5] D. F. Anagnostopoulos *et al.*, Nucl. Instrum. Methods Phys. Res. A **721**, 849c (2003).
[6] M. Trassinelli *et al.*, in *Electron Cyclotron Resonance Ion Sources: 16th International Workshop on ECR Ion Sources ECRIS'04* (AIP, Berkeley, California, 2005), Vol. 749, pp. 81–84, physics/0410250.
[7] N. Nelms *et al.*, Nucl. Instrum. Methods Phys. Res. A **484**, 419 (2002).
[8] M. Hennebach, Ph.D. thesis, Universität zu Köln, 2004.
[9] W. H. Press, S. A. Teukolsky, W. T. Vetterling, and B. P. Flannery, *Numerical Recipes in Fortran 77: The Art of Scientific Computing*, 2nd ed. (Cambridge University Press, New York, 2001).
[10] K. G. Lyon, G. L. Salinger, C. A. Swenson, and G. K. White, J. Appl. Phys. **48**, 865 (1977).
[11] G. Beranger, F. Duffaut, J. Morlet, and J.-F. Tiers, *The Iron-Nickel Alloys* (Lavoisier, Paris, 1996).